IC_{50}=5~8μg/ml を示した（図 10）。次に、HPMA-ZnPP の光照射による細胞毒性増強効果が細胞内の HPMA-ZnPP によるものなのか、細胞外の HPMA-ZnPP によるものかを検討した。光の照射前に、培地を交換または交換せずに光を照射したが、細胞毒性作用に大きな差はなかった（図 10）。HPMA-ZnPP が光照射による細胞毒性効果を示すには、細胞内に取り込まれる必要があると考えられた。

⑤ 光照射による一重項酸素の生成

⑤ - A. 目的

HPMA-ZnPP に光を照射することにより、細胞障害性の高い一重項酸素が生成するかを検討する。

⑤ - B. 方法

一重項酸素の生成は、electron spin resonance（ESR）法により行った。PBS(-)に溶解した 200μg/ml の HPMA-ZnPP 溶液に 30mM の 2,2,6,6-tetramethylpiperidine (TMP)を加え、光照射（キセノンランプ; 400nm~800nm、4.2 J/cm^2 ~ 8.4 J/cm^2）後に ESR スペクトルの測定を行った。ESR スペクトルは JES FA-100（JEOL）を用いて測定した。

⑤ - C. 結果

(図 11) 光照射による一重項酸素の生成

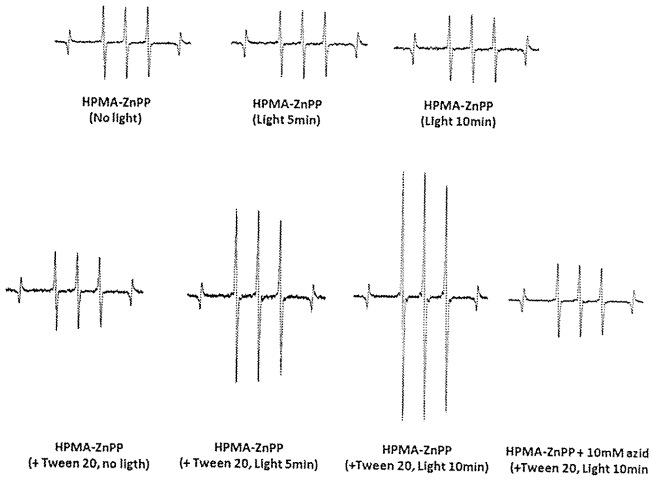

⑤ - D. 考察

一重項酸素（$^1O_2$）の生成は TMP を $^1O_2$ 補足剤とし、electron spin resonance (ESR)法により測定した。HPMA-ZnPP（20μg/ml）の水溶液にキセノンランプ（400nm ~ 800nm）を 14mW/cm^2 の強度で 5~10 分間（4.2 J/cm^2 ~ 8.4 J/cm^2）照射したところ、$^1O_2$ の発生は認められなかった（図 11）。しかし、HPMA-ZnPP に Tween 20 を添加して光を照射したところ、光照射時間に依存して $^1O_2$ の発生が見られた（図 11）。また、シグナルはアジ化ナトリウムにより消失した。これらの結果は、HPMA-ZnPP は水溶液中でミセルを形成しているときは、光を照射しても一重項酸素を発生しないが、界面活性剤などによりミセルが崩壊したときに、一重項酸素を発生することを示唆している。

⑥ レシチンによる HPMA-ZnPP ミセルの崩壊

⑥ - A. 目的

図 11 に示すように、光照射による $^1O_2$ の生成は HPMA-ZnPP のミセル構造が崩壊したときに限定される。また、HPMA-ZnPP の光照射による細胞毒性効果（$^1O_2$ を介した毒性）は、細胞内の HPMA-ZnPP によって引き起こされる（図 10）。これらの結果は、HPMA-ZnPP は細胞内に取り込まれたのちに、ミセルが崩壊し、光照射により $^1O_2$ を放出できる分子状態になっていることを示唆している。レシチンは細胞膜の構成成分であり、両親媒性の物質である。そこで、細胞膜成分により HPMA-ZnPP ミセルの崩壊が促進されるかを検討した。

⑥ - B. 方法

レシチンによる HPMA-ZnPP ミセルの崩壊は、HPMA-ZnPP 由来の蛍光強度を指標とすることにより判定した。ミセルが崩壊すると、ZnPP 由来の蛍光が増強する。10μg/ml の HPMA-ZnPP を 60μg/ml~600μg/ml のレシチンを含む水溶液中でインキュベーションし、経時的に蛍光スペクトルを測定した。

⑥ - C. 結果

(図 12-A) レシチンによる HPMA-ZnPP ミセルの崩壊

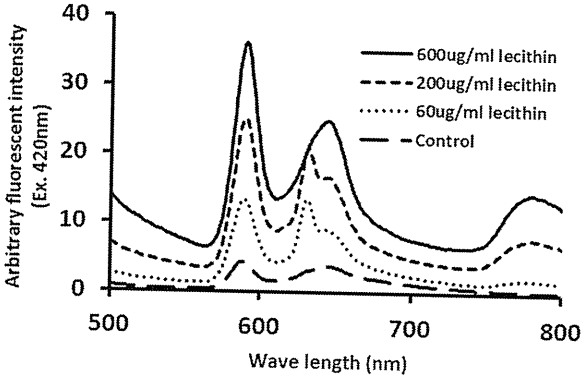

(図 12-B) レシチンによる HPMA-ZnPP ミセルの崩壊

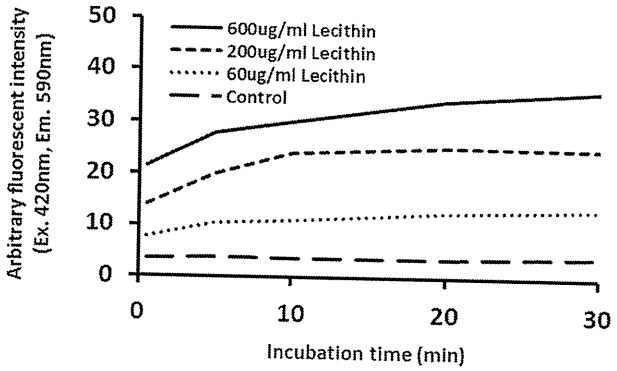

⑥ - D. 考察

HPMA-ZnPP (10μg/ml) をレシチン (60~600μg/ml) と混合し、HPMA-ZnPP ミセルの崩壊を、蛍光を指標として検討したところ、レシチンの用量および時間依存的に、HPMA-ZnPP の蛍光強度の上昇が認められた (Ex. 420nm、Em. 590nm) (図 12A, B)。これらの結果より、HPMA-ZnPP は細胞内に取り込まれたのちに、細胞膜成分により HPMA-ZnPP は崩壊し、光照射により $^1O_2$ を発生し、細胞障害性を発揮すると推察された。

⑦ HPMA-ZnPP の細胞内取り込み

⑦ - A. 目的

HPMA-ZnPP により引き起こされる細胞毒性効果は、①HO-1 の阻害作用または②$^1O_2$ の産生を介したものが考えられる。HO-1 は小胞体局在タンパク質であり、HO-1 の阻害を行うには細胞内に取り込まれる必要がある。また光照射 ($^1O_2$ 産生) による細胞毒性を発揮するためにも、細胞内へ取り込まれる過程が必須となる (図 19-B)。そこで、HPMA-ZnPP の細胞内への取り込みを検討した。

⑦ - B. 方法

HeLa 細胞に ZnPP 当量で 20μg/ml の ZnPP および HPMA-ZnPP を処理し、37℃または 4℃でインキュベーションを行い、経時的に細胞を回収し、細胞内 ZnPP を 95%エタノールで抽出した。蛍光分光光度計を用いエタノール中の ZnPP 由来の蛍光強度を測定した。

⑦ - C. 結果

(図 13-A) HPMA-ZnPP の細胞内取り込み

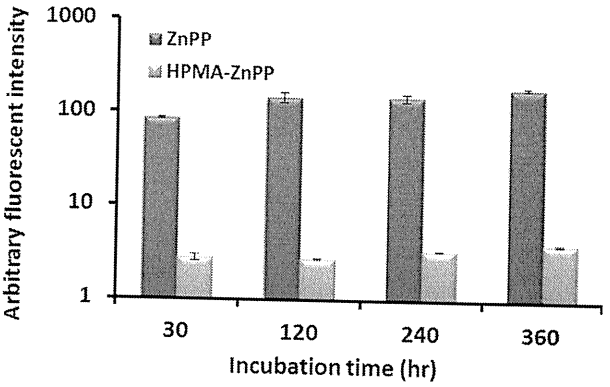

(図 13-B) HPMA-ZnPP の細胞内取り込み

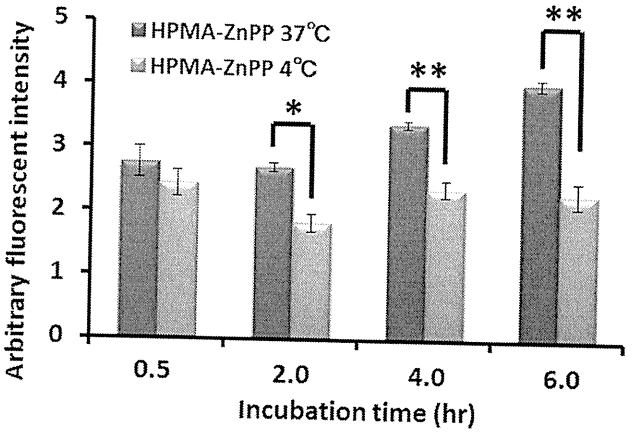

⑦ - D. 考察

HPMA-ZnPP では ZnPP に比べておよそ 40 分

の１程度の細胞内取り込みしか認められなかった(図 13-A)。さらに、HPMA-ZnPP 処理後に 4℃、または 37℃でインキュベーションし、細胞内取り込み量を測定したところ、4℃の培養では、時間依存的な細胞内 HPMA-ZnPP 量の増加が認められなかったことから、HPMA-ZnPP はエンドサイトーシスを介した経路で細胞内に取り込まれていることが示唆された（図 13-B)。図 10-A で見られた、HPMA-ZnPP 単独での細胞毒性効果が見られない理由の一つとして、細胞内取り込みの低さが考えられる。

⑧ HPMA-ZnPP の体内動態

⑧ - A. 目的

担癌マウスにおける HPMA-ZnPP の体内動態を明らかにする。

⑧ - B. 方法

腫瘍径がおよそ 10mm になった S180 担癌マウスに、15mg ZnPP 当量/kg の HPMA-ZnPP を静脈内投与した。投与 24 または 48 時間後にエーテル麻酔により安楽死させ、潅流後に各臓器を摘出した。各臓器を秤量し、1ml/100mg 臓器となるように DMSO を加えた。ホモジナイザーで組織を破砕し、遠心分離（12,000g, 25℃, 10min）することにより、HPMA-ZnPP を抽出した。HPMA-ZnPP 濃度は蛍光強度（Ex. 420nm、Em. 590nm）より定量した。

⑧ - C. 結果

(図 14) HPMA-ZnPP の血中濃度

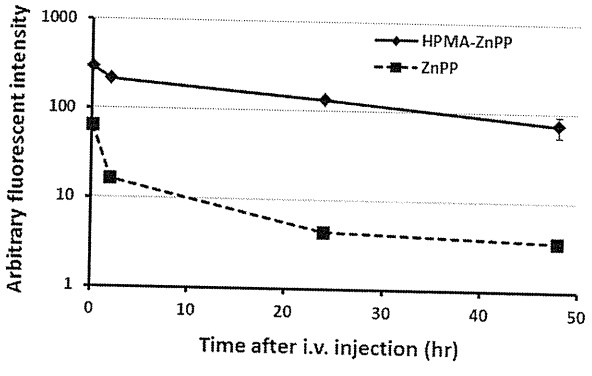

(図 15-A) HPMA-ZnPP の体内動態

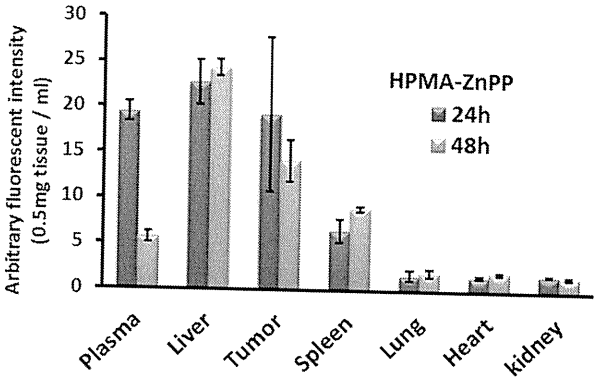

(図 15-B) ZnPP の体内動態

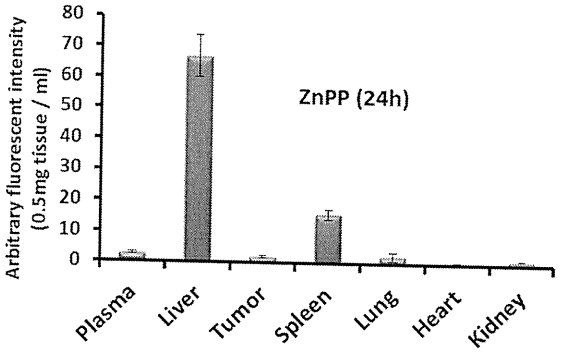

⑧ - D. 考察

ddY マウスに ZnPP 当量で 18mg/kg の ZnPP または HPMA-ZnPP を尾静脈より投与し、経時的に血漿中 HPMA-ZnPP 濃度を定量した。ZnPP は速やかに血中より消失し、投与 2 時間後には投与量の 5%程度しか血中に残存していなかったが、HPMA-ZnPP は 2 時間後ではおよそ 70%、48 時間後でも 25%が血中に見られた（図 14)。次に HPMA-ZnPP の体内分布を検討した。S180 担癌マウスに ZnPP 当量で 15mg/kg の HPMA-ZnPP または ZnPP を尾静脈より投与し、24 および 48 時間後に各臓器中の HPMA-ZnPP または ZnPP 量を定量した。ZnPP 投与では、90%以上が肝臓や脾臓に集積してしまい、腫瘍への分布がみとめられなかった。しかし、HPMA-ZnPP の投与により、投与 24 時間後では、腫瘍濃度は肝臓と同程度、肺、心臓、腎臓に対し 10 倍程度の集積を認めた（図 15-A)。これらの結果により、ZnPP を HPMA-ZnPP とすることにより、EPR 効果により腫瘍集積性が期待されることが明らかとなっ

た。

⑨ HPMA-ZnPP による抗腫瘍効果

⑨ - A. 目的

HPMA-ZnPP が光線力学的療法に利用できるかを検討するため、S180 担がんマウスを用い、光照射併用時における HPMA-ZnPP による抗腫瘍効果を検討する。

⑨ - B. 方法

S180担癌マウスの腫瘍径がおよそ3-5mmになった時に、15mg ZnPP 当量/kg の HPMA-ZnPP を静脈内投与した。光照射はキセノンランプ（400nm~800nm, 6J/cm2）(MAX-303, Asahi spectra)を用い、HPMA-ZnPP 投与 24,48,72 時間後に行った。投与スケジュールは図 22 に示す通りである。腫瘍はノギスを用いて長径 mm（L)、短径 mm（W）を測定し、腫瘍体積（mm^3）= $W^2 \times L / 2$ の計算式により算出した。

⑨ - C. 結果

(図 16)

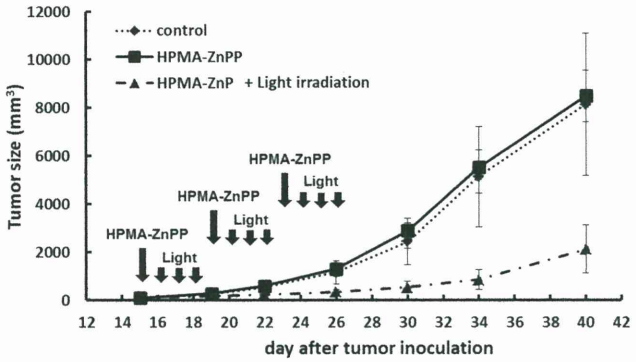

⑩ HPMA-ZnPP による腫瘍イメージング

⑩ - A. 目的

HPMA-ZnPP を腫瘍検出蛍光プローブとして利用できうるのかを検討する。

⑩ - B. 方法

腫瘍径がおよそ 10mm になった S180 担癌マウスに 15mg ZnPP 当量/kg の HPMA-ZnPP を静脈内投与した。投与 24 時間後にマウスの毛を剃毛し、in vivo 発光／蛍光イメージング装置（IVIS XR, Caliper life science）により、蛍光イメージング像を撮影した。HPMA-ZnPP は 430±15nm の光で励起し、695~770nm のバンドパスフィルタを用いて検出した。

⑩ - C. 結果

(図 17-A) 腫瘍蛍光イメージング(HPMA-ZnPP)

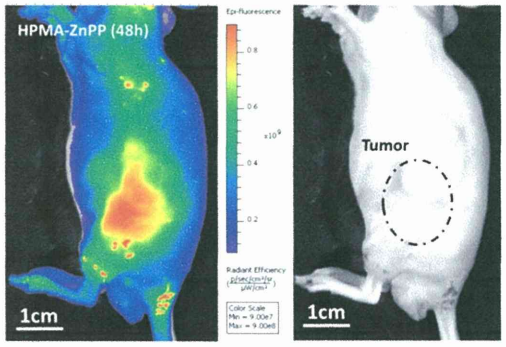

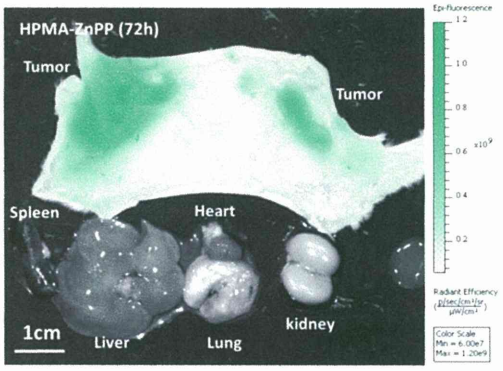

(図 17-B) 腫瘍蛍光イメージング(ZnPP)

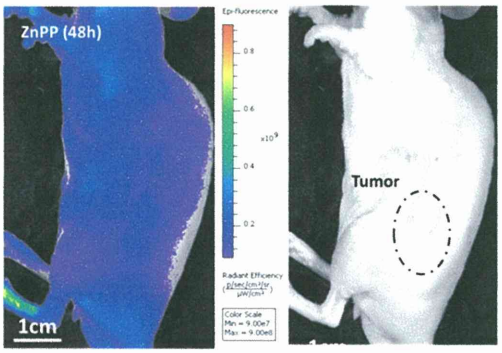

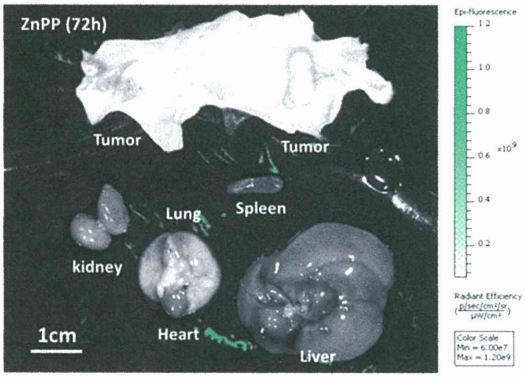

⑩ - D. 考察

HPMA-ZnPP または ZnPP を、担がんマウスに尾静脈より投与後、48 時間または 72 時間後に蛍光イメージングを行った。HPMA-ZnPP を投与したマウスでは腫瘍部特異的に蛍光が認められた。さらに開腹し、臓器を蛍光観察したところ、正常臓器においては蛍光が観察されず、腫瘍組織で強い蛍光が観察された（図 17-A)。ZnPP の投与群においては、腫瘍の蛍光イメージングができなかった（図 17-B）ことから、HPMA-ZnPP とすることで腫瘍選択的に HPMA-ZnPP を集積することができ、腫瘍の蛍光イメージングを可能にできたと考えられる。肝臓や脾臓において蛍光が観察されなかった理由として、ヘムが多く存在している臓器では、ヘムの類縁化合物である ZnPP を励起することができず、蛍光が観察されなかったと思われる。

Ⅱ. 研究発表

1. 論文発表

① J. Fang, H. Nakamura, and H. Maeda, EPR effect: the unique characteristics of tumor blood vessels for drug delivery, factors involved, its limitation and augmentation, **Adv. Drug Delivery Reviews** 63,136-151(2011).

② H. Nakamura, J. Fang, B. Gahininath, K. Tsukigawa, H. Maeda, Intracellular uptake and behavior of two types zinc protoporphyrin (ZnPP) micelles, SMA-ZnPP and PEG-ZnPP as anticancer agents; Unique intracellular disintegration of SMA micelles, **J. Control. Release,** 155, 367-375 (2011).

③ G.Y. Bharate, J. Fang, H. Nakamura, H. Qin, S. Shinkai, and H. Maeda, 4-Amino-6-hydroxypyrazolo [3,4-d] pyrimidine (AHPP) conjugated PEG micelles: Water soluble polymeric xanthine oxidase inhibitor. **J. Drug. Targeting** 19, 954-966 (2011).

④ J. Fang, H. Qin, T. Seki, H. Nakamura, K. Tsukigawa, H. Maeda: Therapeutic potential of pegylated hemin for ROS-related diseases via induction of heme oxygenase-1: results from a rat hepaticischemia/reperfusion injury model. **J. Pharmacol. Exp. Ther.** 339, 779-789 (2011)

⑤ H. Nakamura, J.Fang, H. Maeda. Protective role of D-amino acid oxidase against bacterial infection. **Infection and Immunity**. 80, 1546-1553 (2012)

⑥ G. Bharate, H. Nakamura, J. Fang, S. Shinkai, H. Maeda. Styrene-co-maleic acid (SMA) telomeric micelles encapsulated-zinc protoporphyrin (SMA-ZnPP) and other drugs: Stability study. **CRS Newsletter**, 29,6-7 (2012)

⑦ J. Fang, H. Qin, H. Nakamura, K. Tsukigawa, H. Maeda, Carbon monoxide, generated by heme oxygenase-1, mediates the enhanced permeability and retention (EPR) effect of solid tumor, **Cancer Science** 102, 535-541 (2012)

⑧ H. Nakamura , J. Fang , T. Mizukami , H. Nunoi, H. Maeda, Pegylated D-amino acid oxidase restores bactericidal activity of neutrophils in chronic granulomatous disease via hypochlorite, **Exp. Biol. Med.** (in press)

⑨ H. Maeda, Macromolecular therapeutics in cancer treatment: the EPR effect and beyond, **J. Control. Release** (in press).

⑩ J. Fang, K. Greish, H. Qin, H. Nakamura, M. Takeya, H. Maeda, HSP32 (HO-1) inhibitor, zinc protoporphyrin IX, a water soluble micelle of copoly(styrene maleic acid) as anticancer agent: in vitro and in vivo anticancer effect, **Eur. J. Cancer**, published online (2012)

2. 学会発表

① Nanoparticles of styrene-co-maleic acid telomer (SMA) containing anthracyclin and zinc-protoporphyrin (ZnPP) as new miceller anticancer agents, and SMA conjugate of AHPP, a xanthine oxidase inhibit or for oxystress diseases <Review>, Hiroshi Maeda, Hideaki Nakamura, Gahininath Y. Bharate, Kenji Tsukigawa, Haibo Qin, Jun Fang, International Conference on Biomaterials Science, 2011.3（茨城）

② Evaluation of (styrene-co-maleic acid) telomer micelles encapsulated-zinc protoporphyrin (SMA-ZnPP): A stability study for three different types of SMA micelles, Gahininath Y. Bharate, Hideaki Nakamura, Jun Fang, Bert Klumperma[3], Seiji Shinkai and Hiroshi Maeda, International Conference on Biomaterials Science, 2011.3 （茨城）

③ PEG化亜鉛プロトポルフィリン（PEG-ZnPP）の安定性および腫瘍部位でのPEG鎖切断による細胞内取り込みの改善、月川 健士、中村 秀明、方 軍、新海 征治、前田 浩、第27回日本DDS学会、2011.6（東京）

④ Styrene-co-maleic acid (SMA) telomer micelles encapsulated-zinc protoporphyrin (SZP): Arginine formulation for improved stability and solubility, Gahininath Y. Bharate, Hideaki Nakamura, Jun Fang, Bert Klumperma[3], Seiji Shinkai and Hiroshi Maeda, 第27回日本DDS学会、2011.6（東京）

⑤ The importance of cleavage of PEG chains from pegylated zinc protoporphyrin (PEG-ZnPP) by tumor proteases on intracellular uptake, Kenji Tsukigawa, Hideaki Nakamura, Jun Fang, Hiroshi Maeda, The 38th Annual Meeting & Exposition of the Controlled Release Society, 2011.8（Meryland, USA）

⑥ Stability of styrene-co-maleic acid telomer micelles encapsulated-zinc protoporphyrin (SZP), Gahininath Y. Bharate, Hideaki Nakamura, Jun Fang, Bert Klumperma[3], Seiji Shinkai and Hiroshi Maeda, The 38th Annual Meeting & Exposition of the Controlled Release Society, 2011.8（Meryland, USA）

⑦ 慢性肉芽腫に対するポリエチレングリコール修飾 D-アミノ酸酸化酵素（PEG 化 DAO）を用いた過酸化水素補充療法、中村秀明、水上智之、布井博幸、前田浩、食細胞昨日異常症研究会、2011.12（東京）

Ⅲ. 知的財産権の出願・登録情報

特許出願

発明の名称：高分子型蛍光分子プローブ

国 名：日本

出願番号：特願 2011-193237

出願日：平成 23 年 9 月 5 日

別紙４

研究成果の刊行に関する一覧表

書籍

著者氏名	論文タイトル名	書籍全体の編集者名	書　籍　名	出版社名	出版地	出版年	ページ
H. Maeda	Enhanced permeability and retention effect in relation to tumor targeting.	F. Kratz, P. Senter, H. Steinhagen	Drug Delivery in Oncology. From Basic Research to Cancer Therapy	Wiley-VCH Verlag GmbH & Co. KG,	Weinheim, Germany	2011	Vol.1, 65-84
K. Hochdörffer, G. DiStefano, L. Fiume, H. Maeda, F. Kratz	Liver tumor targeting	F. Kratz, P. Senter, H. Steinhagen	Drug Delivery in Oncology. From Basic Research to Cancer Therapy	Wiley-VCH Verlag GmbH & Co. KG,	Weinheim, Germany	2011	Vol. 3, 1519-1568
H. Maeda	Recollections of 45 years in research: From protein chemistry to polymeric drugs to the EPR effect in cancer therapy		Protein Biochemistry, Synthesis, Structure and Cellular Functions	Nova Science Publishers,	N.Y., USA	2011	1-78

雑誌

発表者氏名	論文タイトル名	発表誌名	巻号	ページ	出版年
H. Maeda, Y. Matsumura	History and impact of EPR effect for the nanomedicine drug developments in cancer chemotherapy	Adv. Drug Delivery Reviews	63	129-130	2011
J. Fang, H. Nakamura, H. Maeda	EPR effect: the unique characteristics of tumor blood vessels for drug delivery, factors involved, its limitation and augmentation	Adv. Drug Delivery Reviews	63	136-151	2011
H. Nakamura, J. Fang, B. Gahininath, K. Tsukigawa, H. Maeda	Intracellular uptake and behavior of two types zinc protoporphyrin (ZnPP) micelles, SMA-ZnPP and PEG-ZnPP as anticancer agents; Unique intracellular disintegration of SMA micelles	J. Control. Release	155	367-375	2011

G.Y. Bharate, J. Fang, H. Nakamura, H. Qin, S. Shinkai, and H. Maeda	4-Amino-6- hydroxypyrazolo [3,4-d] pyrimidine (AHPP) conjugated PEG micelles: Water soluble polymeric xanthine oxidase inhibitor	J. Drug. Targeting	19	954-966	2011
N. Larson, K. Greish, H. Bauer, H. Maeda, H. Ghandehari.	Synthesis and evaluation of poly(styrene-co-maleic acid) micellar nanocarriers for the delivery of tanespimycin	Int'l. J. Pharmaceutics.	420	111-117	2011
J. Fang, H. Qin, T. Seki, H. Nakamura, K. Tsukigawa, H. Maeda	Therapeutic potential of pegylated hemin for ROS-related diseases via induction of heme oxygenase-1: results from a rat hepaticischemia/reperfusion injury model	J. Pharmacol. Exp. Ther.	339	779-789	2011
H. Herrmann, M. Kneidinger, S. Cerny-Reiterer, T. Rülicke, M. Willmann, K.V. Gleixner, K. Blatt, G. Hörmann, B. Peter, P. Samorapoompichit, W. Pickl, G. Y. Bharate, M. Mayerhofer, W. R. Sperr, H. Maeda, P. Valent	The Hsp32 inhibitors SMA-ZnPP and PEG-ZnPP exert major growth-inhibitory effects on $CD34^{+}/CD38^{+}$ and $CD34^{+}/CD38^{-}$ AML progenitor cells.	Current Cancer Drug Targets	12	51-63	2012
H.Nakamura, J. Fang, H.Maeda	Protective role of D-amino acid oxidase against bacterial infection	Infection and Immunity	80	1546-1553	2012
H. Maeda	Vascular permeability in cancer and infection as related to macromolecular drug delivery, with emphasis on the EPR effect for tumor-selective drug targeting	Proc. Jpn. Academy, Series B	88	53-71	2012
G. Bharate, H. Nakamura, J. Fang, S. Shinkai, H. Maeda	Styrene-co-maleic Acid (SMA) Telomeric Micelles Encapsulated-Zinc Protoporphyrin (SMA-ZnPP) and Other Drugs: Stability Study	CRS Newsletter	29	6-7	2012
J. Fang, H. Qin, H. Nakamura, K. Tsukigawa, H. Maeda	Carbon monoxide, generated by heme oxygenase-1, mediates the enhanced permeability and retention (EPR) effect of solid tumor	Cancer Science	102	535-541	2012

H.Nakamura, J. Fang, T. Mizukami, H. Nunoi, H. Maeda	Pegylated D-amino acid oxidase restores bactericidal activity of neutrophils in chronic granulomatous disease via hypochlorite	Exp. Biol. Med			2012 in press
H. Maeda	Macromolecular therapeutics in cancer treatment: the EPR effect and beyond	J. Control. Release			2012 in press
J. Fang, K.Greish, H. Qin, H. Nakamura, M. Takeya, H. Maeda	HSP32 (HO-1) inhibitor, zinc protoporphyrin IX, a water soluble micelle of copoly(styrene maleic acid) as anticancer agent: in vitro and in vivo anticancer effect	Eur. J. Cancer			published online 2012

Edited by Felix Kratz, Peter Senter
and Henning Steinhagen

WILEY-VCH

Drug Delivery in Oncology

From Basic Research to Cancer Therapy

Volume 1

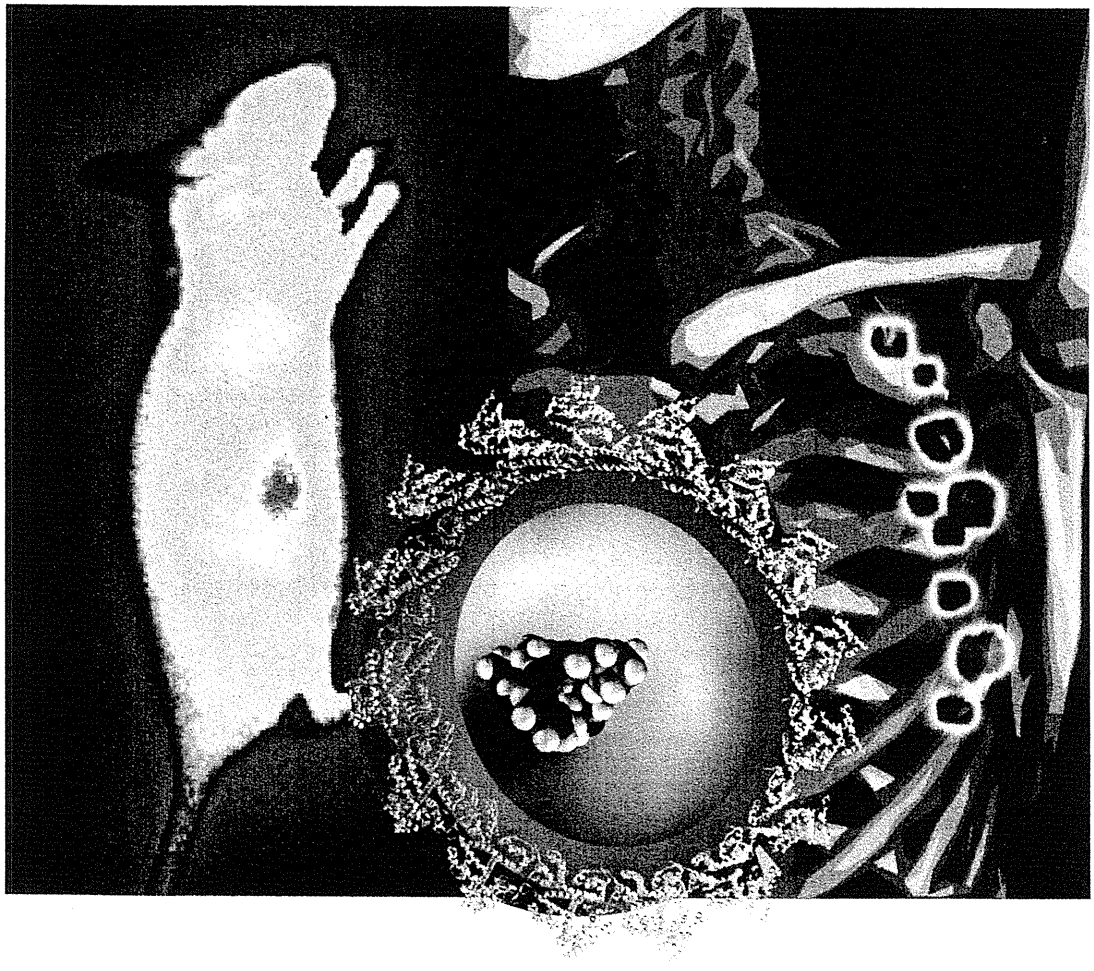

3
Enhanced Permeability and Retention Effect in Relation to Tumor Targeting

Hiroshi Maeda

3.1
Background and Status Quo

We first described the enhanced permeability and retention (EPR) effect of macromolecules in solid tumors under the title of "A new concept for macromolecular therapeutics in cancer chemotherapy: mechanism of tumoritropic accumulation of proteins and the antitumor agent SMANCS" in the December 1986 issue of *Cancer Research* [1]. In prior publications we had described the relationship of plasma half-life of small proteins of about 10 kDa to more than 240 kDa as well as the biocompatibility of proteins in relation to the conformational integrity. For instance, the native versus denatured form of α_2-macroglobulin shows a drastic reduction of plasma half-life when this plasma protease inhibitor of 240 kDa complexes with a protease (trypsin) due to rapid uptake by phagocytotic cells or hepatic entrapment [2–4]. Obviously, inadequate chemical modifications of biocompatible plasma or other proteins will reduce plasma half-life, while appropriate modifications will prolong their half-lives. This effect was noted for the modification of many proteins (e.g., superoxide dismutase (30 kDa) and ribonuclease (12.5 kDa) with divema (divinyl ether–maleic acid copolymer or pyran copolymer), neocarzinostatin (NCS) (12 kDa) with styrene–maleic acid copolymer (SMA) or poly(ethylene glycol) (PEG), etc.) [2–5]. In addition to plasma half-life, two crucial points should be emphasized. Namely, all plasma and other proteins of molecular weight above 40 kDa exhibited tumor-selective accumulation. Thus, we envisaged preferential drug targeting to solid tumors by using macromolecular drugs [1, 2]. We also noted that such macromolecular derivatives accumulated preferentially in the lymphatic tissues [6–8]. The latter point has not received enough attention among oncologists or in the field of cancer chemotherapy, regardless of its importance in relation to lymphatic metastases. Namely, many therapeutic failures in cancer chemotherapy can be attributed to the failure of controlling lymphatic metastases. As a matter of fact, there is no effective treatment for lymphatic metastases, and therapy with common anticancer drugs without lymphotropic accumulation does not control the growth and spread of lymphatic metastases [6–10].

Drug Delivery in Oncology: From Basic Research to Cancer Therapy, First Edition.
Edited by Felix Kratz, Peter Senter, and Henning Steinhagen.

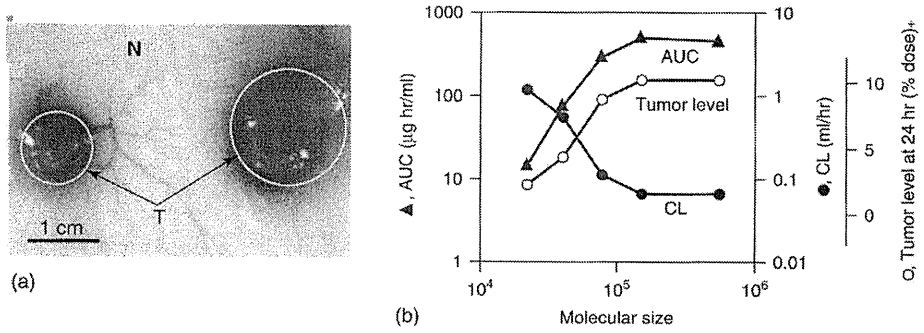

Figure 3.1 (a) EPR effect visualized in experimental mouse tumors where albumin-bound Evans blue (molecular weight 68 kDa) is selectively accumulated only in subcutaneously growing tumor. Arrows 'T' pointing to blue spots are tumors. 'N' is the normal skin that shows no vascular leakage (in contrast to blue-stained tumor). Accumulated Evans blue will remain in the tumor for more than 2–3 weeks. (b) Relation between molecular weight of drugs, plasma level (area under the concentration curve (AUC)), tumor concentration, and renal clearance rate (CL). (Data from [13].)

We have elaborated the EPR effect further by using another biocompatible synthetic polymer, *N*-(2-hydroxypropyl)methacrylamide (HPMA) copolymers, with discrete molecular size distributions, which were supplied by K. Ulbrich (Prague, Czech Republic) [11–14]. All the data are consistent with the concept of EPR effect, and show that polymers with a molecular weight above 40 kDa exhibited prolonged plasma residence time and preferential accumulation of the polymeric or macromolecular drugs in the tumor tissue [11–16] (Figure 3.1).

Meanwhile, the EPR effect is applicable to a wide range of biocompatible macromolecules, such as proteins/antibodies, liposomes, micelles, DNA or RNA polyplexes, nanocarriers, and lipidic particles for cancer-selective drug delivery [13–16]. The number of papers that cite the EPR effect has increased in a logarithmic manner in recent years, reaching close to 8000 in 2010 (Figure 3.2). In this chapter, I will review the EPR effect briefly, and discuss problems/limitations, solutions, and further augmentation of the EPR effect.

3.2
What is the EPR Effect: Mechanism, Uniqueness, and Factors Involved

The EPR effect is a phenomenon resulting from multiple causes and effects, such as anatomical defects in vascular architecture and higher vascular density as a result of active production of angiogenic factors, especially when tumors are at an early stage and express growth factors such as vascular endothelial growth factors (VEGFs) and nitric oxide (NO). Many vascular permeability factors such as NO (Figure 3.3a–c), bradykinin, prostaglandins, collagenases, matrix metalloproteinases (MMPs), and so on, are overproduced in the tumor tissues (Tables 3.1 and 3.2). They facilitate extravasation of macromolecules in solid tumors [11–21]. As a result, more excessive tumor-selective vascular leakage of

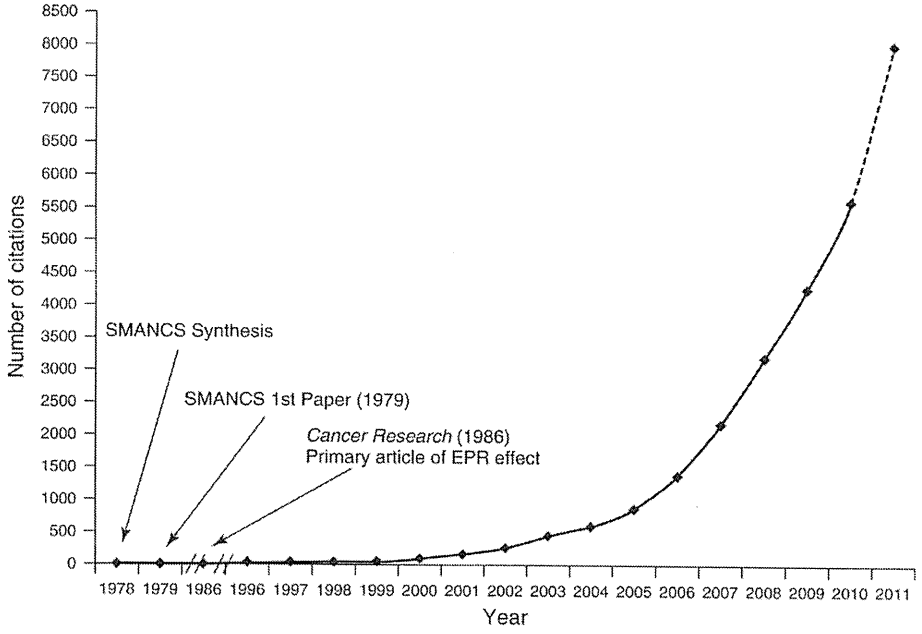

Figure 3.2 Citation numbers of the EPR effect and invention of the first polymeric drug, SMANCS (from *Science Direct* and *SciFinder*). (Adapted from [16].)

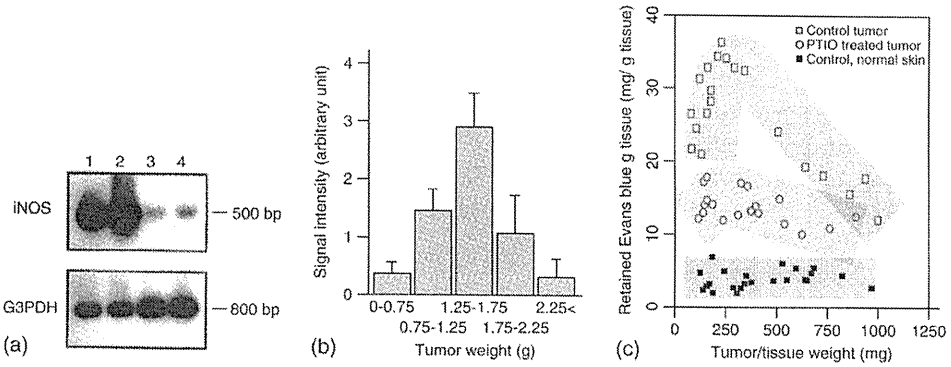

Figure 3.3 (a)–(c) Involvement of NO in the EPR effect: nitric oxide synthase (NOS) induction, relation to tumor size, and effect of NO scavenger by tumor size. (a) Upregulation of the inducible form of NOS (inducible nitric oxide synthase, iNOS) in tumors (lanes 1 and 2) and normal tissues (lanes 3 and 4). (b) Amount of NO generated in solid tumor (S-180) in mice as measured by electron spin resonance spectroscopy with dithiocarbamate–Fe complex and the relation to the size of tumor. (c) Amount of Evans blue–albumin permeation (EPR effect) and effects of NO scavenger (2-phenyl-4,4,5,5-tetramethylimidazolineoxyl-1-oxyl-3-oxide (PTIO), ○) or NOS inhibitor (■) in mouse tumors based on tumor size. Lower zone: control normal tissue; middle zone: treated with PTIO; top zone: control tumor, without NO scavenger. (Adapted from [16, 19].)

Table 3.1 Factors affecting the EPR effect of macromolecular drugs in solid tumors (extensive production of vascular mediators that facilitate extravasation).

Bradykinin
Nitric oxide (NO)
Vascular permeability factor/VEGF
Prostaglandins
Collagenase (MMPs)
Peroxynitrite ($ONOO^-$)
Anticancer agents
Inflammatory cells and H_2O_2
Heme oxygenase-1 (CO)

Table 3.2 Architectural differences and functions.

1) Active angiogenesis and high vascular density
2) Defective vascular architecture
lack of smooth muscle layer
lack of or fewer receptors for angiotensin II
large gap in endothelial cell–cell junctions and fenestration
anomalous conformation of tumor vasculature (e.g., branching or stretching)
3) Defective lymphatic clearance of macromolecules and lipids from interstitial tissue (prolonged retention of these substances)
4) Whimsical and bidirectional blood flow

an albumin-bound dye such as Evans blue will occur only at the tumor site, as seen in the examples shown in Figure 3.1a. The uniqueness of this phenomenon is that it will be only seen in tumor tissues, but not in the normal healthy tissue [11, 13–20]. Obviously, normal vasculatures shows no such leakage (Figures 3.1a and 3.3a and c) due to their complete architecture of the blood vasculature as well as little production of vascular mediators as listed in Table 3.1.

Furthermore, macromolecules with a molecular weight more than 40 kDa above the renal threshold such as synthetic polymers, serum proteins, micelles, polymer-based or lipid-based nanoparticles that leak out of the blood vasculature into the interstitial space of tumor tissues remain there for a very long time, even for several weeks, without being cleared (Figures 3.1a,b 3.4, 3.5, and 3.9b) [1, 13, 15]. In contrast to tumors, such micro- or nano- particles, should they leak out of the blood vasculature into normal tissue, will be cleared gradually by the lymphatic system in several days as is usually seen for common inflammations of normal tissue. Neovasculature generated by the tumor is characterized by an irregular shape, dilated, leaky, or defective vessels. The endothelial cells are poorly aligned or disorganized with large fenestrations as illustrated for healthy and tumor vessels in Figure 3.4.

These anatomical features make the vasculature of tumor tissue permeable for macromolecules or even larger nanosized particles such as liposomes or polymeric micelles, whereas in blood vessels of healthy tissue only small molecules can pass

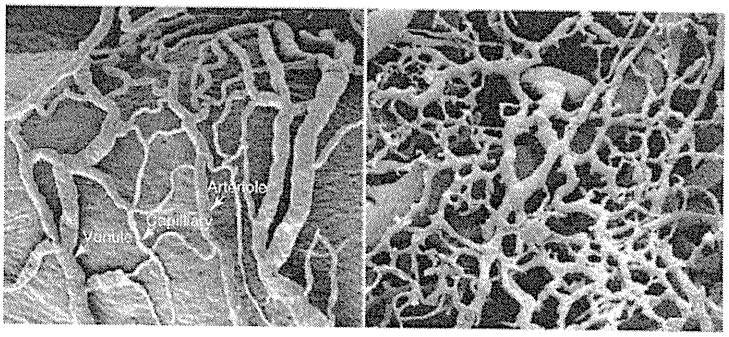

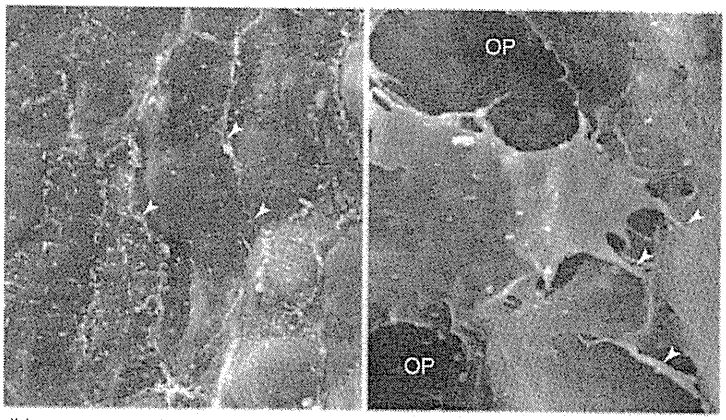

Figure 3.4 (a) Scanning electron microscopy (SEM) imaging of polymer casts of normal (vasa vasorum of rat carotid sinus, left) and tumor (xenograft of human head and neck cancer in nude mouse, right) microvasculature. Marked differences are found in the degree of organization and an apparent lack of conventional hierarchy of blood vessels of the tumor sample. (b) SEM images of the luminal surface of healthy (mouse mammary gland, left) and tumor (MCa-IV mouse mammary carcinoma, right) blood vessels. While the healthy vessel is smooth and has tight endothelial junctions (arrow heads), the tumor vessel shows widened intercellular spaces, overlapping endothelial cells (arrow heads), opening (OP) and other abnormalities. (Reproduced with permission from [22].)

the endothelial barrier. The pore size of tumor microvessels was reported to vary from 100 to 1200 nm in diameter (depending on the anatomic location of the tumor). In contrast, the tight junctions between endothelial cells of microvessels in most normal tissues are less than 2 nm in diameter (noteworthy exceptions are found in postcapillary venules (up to 6 nm), and in the kidneys, liver, and spleen (up to 150 nm)) Figure 3.4b.

The EPR effect is depicted schematically in Figure 3.5.

Figure 3.5 illustrates that blood vessels in most normal tissues have an intact endothelial layer that allows the diffusion of small molecules, but not the entry of

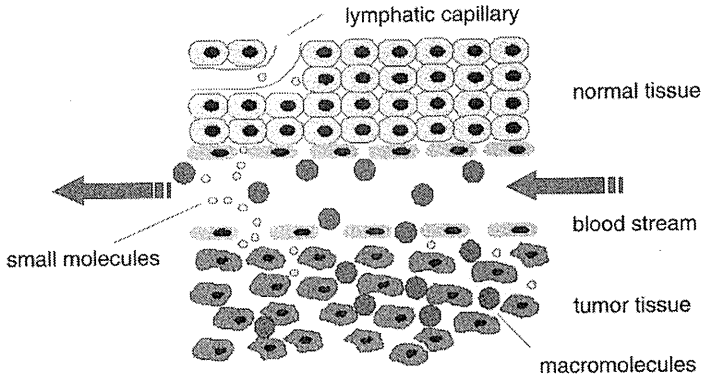

Figure 3.5 Schematic representation of the anatomical and physiological characteristics of normal (upper half) and tumor (lower half) tissues with respect to the vascular permeability and retention of small (lighter circles) and large molecules (darker circles) (see text) [23].

macromolecules into the tissue. In contrast, the endothelial layer of blood vessels in tumor tissue is often leaky so that small as well as large molecules have access to malignant tissue. As tumor tissue does not generally have a lymphatic drainage system, macromolecules are thus retained and can accumulate in solid tumors.

As described above, we can demonstrate this retention effect by injecting Evans blue intravenously, which binds with high affinity and selectivity to the plasma protein albumin (66.5 kDa), and remains in circulation for more than several hours in rodents.

During the long circulation time of Evans blue bound to albumin, the albumin–Evans blue complex will eventually permeate through the porous tumor blood vessels into the interstitial tissue of tumor, thus staining the tumor blue (Figure 3.1a, 3.5). Alternatively, by infusing a lipid contrast agent such as Lipiodol® with/without the polymeric anticancer drug SMANCS (a conjugate of SMA and NCS) via the tumor-feeding arterial route, Lipiodol will be taken up most effectively by the tumor (Figure 3.6a,c and 3.7). In this case, the ratio of the concentration of Lipiodol in the tumor to circulating blood is more than 2000-fold, translating into an extremely tumor pin-pointed targeted delivery [24–26]. When X-ray computed tomography (CT) scans are taken 1 or 2 days after Lipiodol infusion, one can visualize the white Lipiodol-stained tumor areas showing tumor-selective extravasated areas (Figure 3.7a). In this setting, the lipophilic polymeric drug SMANCS dissolved in Lipiodol (thus named SMANCS/Lipiodol) is retained in the tumor tissue selectively. The presence of Lipiodol and SMANCS can be detected as high-election-density areas ("white areas") due to iodine in Lipiodol using X-ray imaging [14, 24–26].

This method allows detection of tumor nodules as small as a few millimeters in diameter [24, 25]. Furthermore, this prolonged retention in tumor tissue is more than just a passive targeting. Namely, when a low-molecular-weight water-soluble contrast agent is infused under identical conditions (known as angiography)

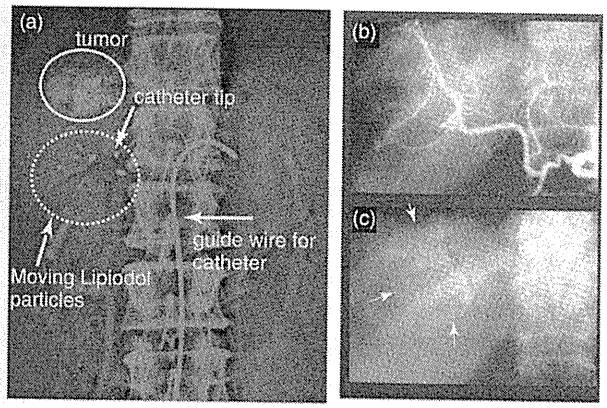

Figure 3.6 (a) Angiographic arterial infusion of SMANCS/Lipiodol using a catheter (Seldinger method) via the hepatic artery (where vascular leakage is seen, but only within 1 min). White Lipiodol particles coming out are captured at the tumor. (b) Arterial phase (blood vessels are visible). (c) Venous phase.

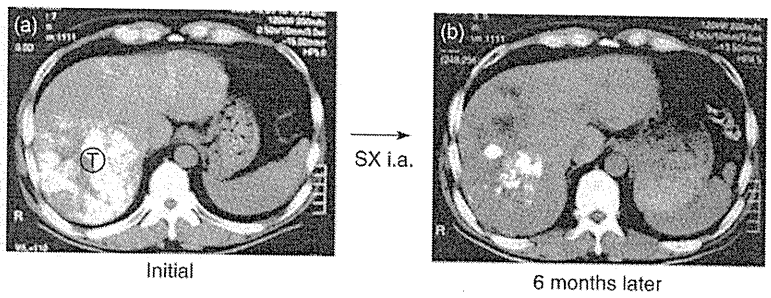

Figure 3.7 X-ray CT scan images of hepatocellular carcinoma (hepatoma) of a patient, where tumor location 'T' and size are visualized by white staining of high-electron-density iodine in the radio contrast agent Lipiodol, which is selectively retained in the tumor. (a) CT image at the first injection. (b) Significant size reduction of the tumor is seen after 6 months of arterial injection of SMANCS 3 times in 6 months via the hepatic artery.

(Figure 3.6a and b) it allows visualization of a solid tumor with the aid of X-ray imaging. However, this tumor staining lasts for only 1–5 min as illustrated by venous-phase staining images (e.g., Figure 3.6c). In contrast to this short time of duration, lipid particles (e.g., Lipiodol) or polymeric drugs, or albumin-bound Evans blue are retained for significantly longer time periods as a result of the EPR effect. The prolonged retention of macromolecules and nanoparticles in the tumor continues for days to weeks, and if they carry a drug this can be released in the vicinity of tumor cells. When an adequate concentration of the active drug in the tumor tissue is attained, it will lead to definite tumor regressions [27]. Thus, the EPR effect is an event observed in *in vivo* settings, but not *in vitro* or cell-free systems, not to mention in normal tissues.

In this context, it may be worth mentioning the enhanced vascular permeability of inflammatory tissues. The enhanced vascular permeability of a tissue is one of the hallmark manifestations of inflammation, which may also involve bradykinin, reactive oxygen species, and other mediators. We had initially observed that bacterial proteases induce activation of a bradykinin-generating cascade [28–32]. Similar events were also discovered in cancer tissues [20, 21, 29–32]. Activation of the kallikrein–kinin cascade leads to the generation of bradykinin that will potentiate the EPR effect instead of suppressing the EPR effect. Another effect is the heterogeneous tumor cell growth with unparalleled angiogenesis resulting in inadequate supply of oxygen (i.e., low pO_2), which will affect induction of p53 or other events that will lead to apoptosis signaling, including the disappearance of vasculature or apoptotic/necrotic tissue death.

If the tumor tissue retained normal or near normal innate immunity such as macrophage functions, it would exert defensive a host response generating NO and superoxide (O_2^-). Both of them react immediately to become peroxynitrite ($ONOO^-$) at confined local vicinities, where $ONOO^-$ is highly toxic and exerts oxidative and nitrating effect, and affects cancer cells [29]. In addition to the cytotoxic effect of $ONOO^-$ (and ClO^-), $ONOO^-$ can activate MMPs (or collagenases) that disrupt tissue matrices and vascular integrity, and facilitate vascular leakage (i.e., the EPR effect) [19, 20, 29, 33]. (The $ONOO^-$ thus generated modifies tyrosine to form nitrotyrosine and guanine to form 8-nitroguanine in nucleic acid as well as 8-nitrocylic GMP [34, 35]. 8-Nitroguanosine becomes a substrate of NADPH-dependent reductase such as cytochrome b_5 reductase and iNOS [36, 37]. As a matter of fact, one can demonstrate the presence of nitrotyrosine and 8-nitroguanosine in tumor cells (by fluorescence immunostaining and high-performance liquid chromatography). The cell-killing potency of $ONOO^-$ is as strong as hypochlorite (ClO^-; i.e., below 10 μM), which is another reactive chemical produced by leukocytes (neutrophils) from H_2O_2 and Cl^- by myeloperoxidase [29].) Tumor tissues under these circumstances are therefore heterogeneous or different from normal pathophysiological tissue.

These vascular effectors that are common among cancer and inflammatory tissues open up the endothelial cell–cell junction, and allow proteins and macromolecules to extravasate into the interstitial tissue. However, they will be gradually recovered via the lymphatic clearance system in a matter of a few to several days. In contrast to this phenomenon of normal tissue, the clearance of drug nanoparticles or drug polymer conjugates from cancer tissue is much slower, and results in sustained access of this type of polymer therapeutics to cancer cells, which is the most desired goal in cancer drug delivery.

3.3
Heterogeneity of the EPR Effect: A Problem in Drug Delivery

The EPR effect is universally observed in rodent, rabbit, and human solid tumors. It is more typical when the tumor size is less than 1 cm. However, as shown in Figure 3.8a–c, when a tumor grows larger than 1 cm, the tumor exhibits more heterogeneity in the EPR effect. Yet it is seen even when tumor nodules are as

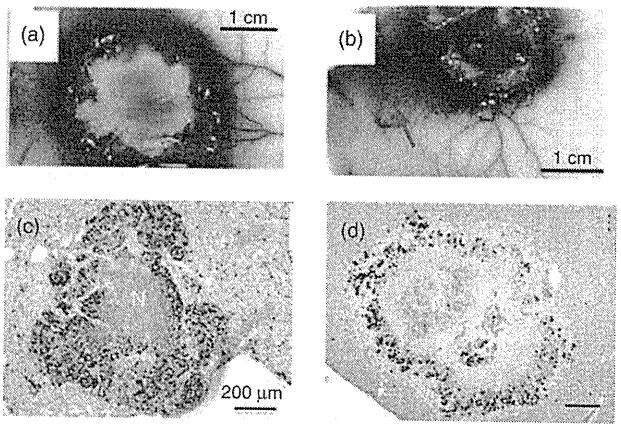

Figure 3.8 Heterogeneity of the EPR effect as seen by extravasation of Evans blue–albumin in tumor. (a) and (b) S-180 tumor in mouse. Macroscopic tumor and the skin, after intravenous Evans blue injection. In both (a) and (b), the tumor tissue shows heterogeneous staining of Evans blue as inhomogeneous extravasation of the blue dye–albumin complex. This type of peripheral uptake of SMANCS/Lipiodol is seen via CT in metastatic human tumors and is classified as B-type staining (26). Arrows in (a) and (b) point to areas in which the EPR effect also occurs in normal tissue as a result of the generation of vascular mediators such as bradykinin. This extravasated blue albumin in normal skin will be cleared via the lymphatics. Ki-67 immunohistochemistry was used to assess tumor proliferation in (c) and (d). Proliferating cells were demarcated by intense brown diaminobenzidine staining in (c). In (d), polymeric drug SMA–pirarubicin reduced tumor proliferation by greater than 75% in 72 h after one intravenous injection. Control tumors of (c) demonstrated a high degree of tumor proliferation. Tumor proliferation was restricted to a thick viable band at the tumor periphery with significant central necrosis (N). (d) Proliferation in SMA–pirarubicin-treated tumors was restricted to the thin viable rim at the tumor periphery. Scale bars = 200 μm [38].

small as 0.5 mm in diameter in metastatic micronodules of the liver (Figure 3.8c,d), although tumor-selective extravasation of a polymeric drug (by the EPR effect) can be observed (Figure 3.9b). In the metastatic liver cancer model of colon cancer, the microheterogeneity of the EPR effect is also observed as viable parts and necrotic parts near the center of the tumor (Figure 3.8c) [38]. However, it should be noted that the tumor-proliferating area is located primarily at the periphery of the solid tumor, which coincides with the area showing an extensive EPR effect, while a hypovascular or avascular appearance is seen in the tumor center (Figures 3.8a and c and 3.10a and b). Despite the heterogeneity of the EPR or the vasculature of the tumor, macromolecular drugs show much more drug accumulation by EPR in the tumor periphery where more proliferating tumor cells exist (see peripheral staining in Figures 3.8a and c and 3.10a,b).

Therefore, the area with a high EPR effect coincides with the tumor growth area. Thus, using cytostatic polymeric drugs is more advantageous from the therapeutic point of view since they act effectively on proliferating cancer cells. In this context, 90–95% suppression of metastatic tumor nodules in the liver by

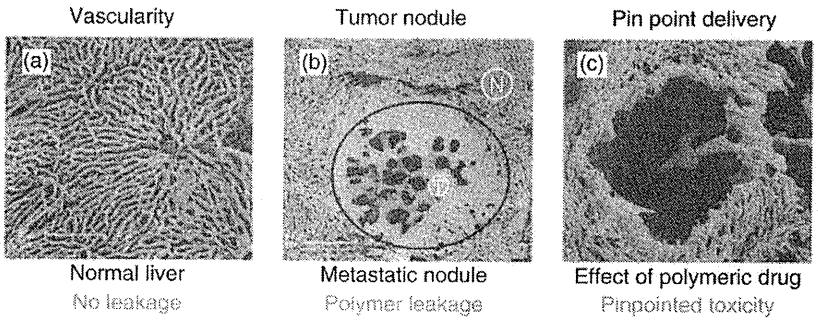

Figure 3.9 SEM images of metastatic colon cancer to the liver. (a) Normal liver vessels. (b) Metastatic micronodule of tumor indicating by 'T' (blood bed) where polymeric resin is extravagated by the EPR effect. (c) After a treatment of tumor-selective polymeric drug (SMA micelles with pirarubicin) by intravenous injection. The nodular blood bed of the metastatic tumor has disintegrated: tumor tissue has undergone apoptosis and necrosis by tumor-selective drug delivery; however, no damage to the normal liver tissue is seen. More than 95% of tumor nodules in the liver are destroyed by this drug given intravenously. The images are courtesy of Dr. J. Daruwalla and Professor C. Christophi of the University of Melbourne, Australia [38].

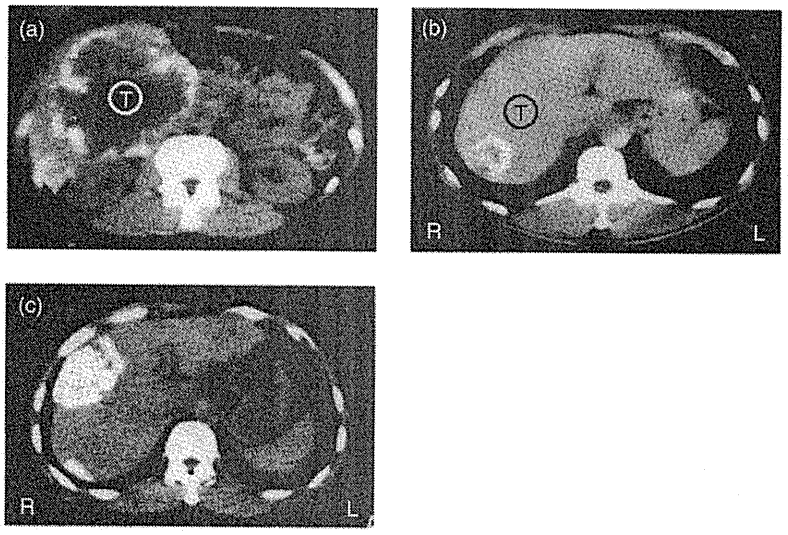

Figure 3.10 X-ray CT scan of the liver cancer after SMANCS/Lipiodol injection via the arterial route under normotensive blood pressure. Heterogeneity of drug uptake in (a) and (b) is remarkable as a ring-like staining. Namely, an avascular or hypovascular area is noted as a dark area in the central part of metastatic liver cancer (a), a massive size metastasized tumor from the gallbladder, and (b) metastatic liver cancer from the colon. In (c), primary liver cancer (hepatocellular carcinoma) seen as a white area at the right side of the liver lobe in the CT image where uptake of SMANCS/Lipiodol is homogeneous.